Zhao Bo

College of Textiles,
Zhongyuan University of Technology,
Henan, Zhengzhou, 450007,
People's Republic of China

Experimental Study and Numerical Analysis for Prediction of the Fibre Diameter of Polylactic Acid (PLA) Spunbonded Nonwovens

Abstract
An air-drawing model of the polylactic acid (PLA) spunbonding process is presented and solved by introducing numerical computation results of the air jet flow field of an aerodynamic device. At the same time, the model is also verified by experimental results obtained with our university's equipment. The influence of the density and specific heat capacity of polymer melt at a constant pressure changing with the polymer temperature on the fibre diameter was studied. The fibre diameters predicted is in good agreement with experimental data. The effects of processing parameters on the fibre diameter are further analysed. We find that a lower polymer throughput rate, a higher initial temperature of the melt,a higher initial temperature, velocity, and suction speed of the air can all produce finer fibres, but during the incruse in the venturi gap, the fibre diameters first decrease and next increase again. The results encourage us to further investigate how fine a fibre diameter can be obtained in the spunbonding process and what factors influence the fibre diameter formed. Furthermore, the results also show the great perspective of this research in the field of the (CAD), of the spunbonding process and technology.

Key words: *polylactic acid, spunbonding, nonwovens, fibre diameter, air-drawing, computer modeling.*

Designations used

- Q - *polymer mass flow rate, kg/s.*
- D - *filament fibre diameter, mm.*
- V - *filament fibre velocity, m/s.*
- V_a - *air velocity, m/s.*
- g - *gravitational acceleration, g/s^2.*
- C_{pf} - *specific heat capacity of melt, J/(kg·K).*
- h - *convective heat transfer coefficient, W/m^2·K*
- T - *polymer temperature,*
- T_a - *the air temperature,*
- j - *sign carrier of the air drag force, when j is -1 for $v_a > v$ and 1 for $v_a < v$.*
- C_f - *coefficients of air skin friction drag.*
- Re - *the Reynolds number.*
- ρ_f - *polymer density, kg/m^3.*
- ρ_a - *air density, kg/m^3.*
- η - *the shear viscosity of air, Pa·s*

Introduction

Dating back to the 1950's, spunbonding technology is a one step process to make nonwovens directly from thermoplastic polymers with the aid of high velocity and cool air to attenuate the polymer melt filament fibre [1 - 4]. The spunbonded web is ideally suited for medical, roof, hygienic materials [5 - 6], and so on. Typical polymer resins used include polypropylene (PP) and polyester, which are the most widely used polymers for the nonwoven spunbonding process, others such as polyethylene (PE), polyethylene terephthalate (PET), and polyamide (PA) can also be used to produce spunbonded nonwoven webs. However, nowadays more and more people are conscious of environmental protection, thus it is very important to study environmentally friendly products. polylactic acid (PLA) nonwovens are just such products [6 - 12]. The processing of polylactic acid (PLA) nonwovens is still at the development stage as its rheological behaviour is restrictive for such application [13 - 17]. PLA nonwoven products have many good properties in comparison with polyethylene terephthalate: the melting point and glass temperature of PLA are low; it is entirely derived from a renewable resource, currently from corn; and it can be biodegraded after use. Spunbonded nonwovens are self-bonded with no chemical binders, therefore all these features mean that PLA can produce spunbonded nonwovens fabrics which are entirely environmentally friendly. Hence it can be positively stated that PLA is suitable for spunbonded nonwoven technology. The polymer flow behaviour is, however, not quite the same for different kinds of polymers because of their different shear viscosity and constitutive equations. To determine whether the air drawing model can be used for predicting the fibre diameter of the PLA polymer, many studies similar to our previous ones have been devoted to the theoretical and experimental investigation of spunbonding. In this study, we concentrated specifically on polylactic acid (PLA) polymer. In this paper, an air drawing model of the polymer will be established based on the numerical computational method, and the numerical results will be verified with experimental data obtained with our university's equipment. At the same time, we also consider the effects of the variation in the polymer processing parameters and further study the effects of spunbonding process parameters on the fibre diameter. Based on the new air drawing model in the spunbonding process, one further improvement will be made to the model in this work**:** considering the influencesfibre of the variation in the density and specific heat capacity of the polymer melt at a constant pressure changing with the polymer temperature on the fibre diameter. The final fibre diameter can then be predicted with the help of this air drawing model. It is found that the model can be applied to predict drawing effects successfully. The effects of the processing parameters on the fibre diameter will also be investigated by utilising the air drawing model [19 - 21]. The results also reveal the great potential of this research to be used in the computer-aided design (CAD) of spunbonding processes, technology and equipment.

Zhao Bo; Experimental Study and Numerical Analysis for Prediction of the Fibre Diameter of Polylactic Acid (PLA) Spunbonded Nonwovens.
FIBRES & TEXTILES in Eastern Europe 2009, Vol. 17, No. 5 (76) pp. 82-86.

Air drawing model of the polymer with reference to PLA

Our air-drawing model of PLA polymer consists of a continuity equation, a momentum equation, an energy equation, a crystallisation kinetics equation, and a constitutive equation [18 - 29]. The surrounding air conditions (velocity and temperature) are considered as given functions of the axial position and obtained by numerical simulation. In the literature [22, 28, 34], the density ρ_f and specific heat capacity of polymer melt at constant pressure C_{pf} are considered to be constant; in fact, they vary with the polymer temperature T. In this work, we establish an air drawing model that differs from the others given in the citations above and consider the effects of the variation in the density and specific heat capacity of the polymer at a constant polymer temperature. Because the air velocity and temperature are obtained by numerical solution of the air jet flow field of the spunbonding drafting assembly, we can predict the drawing effects with the aid of this air drawing model.

Continuity equation

$$Q = \pi/4\, D^2 V \rho_t \tag{1}$$

where Q is the polymer mass flow rate, D is the filament fibre diameter, V is the mean velocity in the spinning direction, and ρ_t is the specific density of the polymer (this quantity depends on temperature). As the polymer density varies with the polymer temperature, the following correlation [30] is also introduced**:**

$$\rho_t = \frac{1}{1.145 + 0.000903 \times T} \tag{2}$$

where T is the polymer temperature.

Momentum equation

$$\frac{dF_{rheo}}{dz} = \frac{\pi}{2} j \rho_a C_f \left(V_a - V\right)^2 D + \\ + Q\frac{dV}{dz} - \rho_f \frac{\pi}{4} D^2 g \tag{3}$$

where F_{rheo} is the rheological force, z the spinning axial position, ρ_a the air density, j is sign carrier of the air drag force when j is -1 for $V_a > V$ and 1 for $V_a < V$, ρ_f the polymer density, V the filament fibre velocity, V_a the air velocity (the drag results from friction between the filament fibre and air when the two are moving at different velocities, because the high air suction in the chamber results in high axial air velocities, therefore, the relative velocity is used in the term instead of the actual velocity of the filament fibre), g is the gravitational acceleration, and C_f is the air drawing coefficient, which will vary with the axial position. C_f was given by Matsui [31] with the following correlation:

$$C_f = \beta \cdot (Re_d)^{-n} \tag{4}$$

where Re_d is the Reynolds number based on the diameter of the fibre, and β & n are fitted constants; the values of β and n should be 0.37 and 0.61, respectively, as far as the spunbonding process is concerned. The empirical relationship expression of the Reynolds number is as follows**:**

$$Re_d = \rho_a D|(V_a - V)|/u_a \tag{5}$$

Where ρ_a is the density of air, $(V_a - V)$ the relative velocity between the moving filament fibre and air, and u_a the viscosity of air.

Energy equation

$$\frac{dT}{dz} = -\frac{\pi D h \left(T - T_a\right)}{Q C_{Pf}} + \frac{\Delta H_f}{C_{Pf}} \frac{dX}{dz} \tag{6}$$

where T is the filament fibre temperature, T_a the air temperature, h the heat transfer coefficient, which will vary with the axial position, C_{Pf} the specific heat capacity of the polymer melt, which will vary with temperature at a constant pressure, ΔH_f the heat of the fusion of the polymer and X the degree of crystallinity. The first term on the right-hand side of equation 6 describes the decrease in temperature due to heat loss by the fibre to the cooling medium, whereas the second term represents the opposite effect that crystallisation has on temperature due to the release of the latent heat of fusion. The value of the heat transfer coefficient can be calculated from the following relation between Nu and Re_d.

$$Nu = \gamma\, (Re_d)^m \tag{7}$$

$$h = Nu \cdot K_a / \mathrm{D} \tag{8}$$

where Nu is the Nusselt number at a position based on the filament fibre diameter, K_a the air heat conduction coefficient, and γ & m are empirical constants. The values of γ and m assumed are 0.42 and 0.334, respectively.

Like polymer density, the correlation of the specific heat capacity at a constant pressure of the polymer melt changing with the polymer temperature [30] is as follows**:**

$$C_{Pf} = 0.3669 + 0.00242 \times \mathrm{T} \tag{9}$$

Constitutive equation

As is commonly known, the polymer melt used in the spunbonding process is a kind of non-Newtonian fluid; however, with the simplest constitutive equation, A Newtonian fluid relationship is used in this work because research shows that the temperature dependence on viscosity is the most dominant effect, while the type of constitutive equation is secondary [32 - 33]; therefore, for the sake of computational simplicity, a Newtonian fluid constitutive equation is introduced in our model**:**

$$F_{rheo} = \frac{\pi}{4} D^2 \eta \frac{dV}{dz} \tag{10}$$

Where η is the shear viscosity, i.e. the change in air velocity and temperature with the position in the spinline.

Crystallisation kinetics equation

The variation in the degree of crystallinity along the spinline is given by the following equation.

$$\frac{d}{dz}\left(\frac{X}{X_\infty}\right) = \frac{n_1 k}{V}\left(1 - \frac{X}{X_\infty}\right)\left[\ln\left(1\Big/\left(1 - \frac{X}{X_\infty}\right)\right)\right]^{\frac{n_1 - 1}{n_1}} \tag{11}$$

where $X\infty$ is the maximum crystallinity, $X/X\infty$ is the relative crystallinity, the ratio of the absolute crystallinity to the ultimate crystallinity of the material, n_1 the Avrami index and k the crystallisation rate. Further details about the n_1 and k can be found in the literature [34].

Boundary conditions

$$V(0) = V_0,\ F(0) = F_0,\ D(0) = D_0, \\ X(0) = 0,\ T(0) = T_0,\ F_{rheo}(L) = 0 \tag{12}$$

Here L is the chamber length, F_0 the initial rheological force of the polymer melt, V_0 the initial velocity of the polymer melt, D_0 the initial diameter of the polymer melt, and T_0 is the initial temperature of the polymer melt.

The "freezing-point" is defined as the boundary condition. The method used for determining the initial rheological force F_0 is the searching "freezing-point" method, which requires checking whether the fibre diameters before and beyond a certain "point" along the filament are equal to each other when F_0 is considered to be the sum of the cumulative gravitational and air drawing force acting upon the frozen part of the filament fibre. If the fibre diameters are found to be the same, the "point" is the so-called "freezing-point", in which an appropriate initial rheological force is used.

Dynamics balance equation

$$F = F_{asp} + F_{grav} - F_{drag} - F_{inertia} \quad (13)$$

where F is the force on the filament fibre, F_{asp} the tension exerted by the aerodynamic drawing device, F_{grav} the gravitational force, F_{drag} the air drag on the filament fibre, and $F_{inertia}$ the inertial force.

Experimental procedure

Material structure and characterisation

PLA is perpendicular crystal determined by means of an electric microscope and X ray diffraction; the crystal parameters are as follows: a = 1.078 nm, b = 0.604 nm, c = 2.87 nm, with every crystal consisting of 20 units. The T_m of PLA is 130 ~ 170 °C and T_g is 50 ~ 60 °C. Like other polymers, the characteristics of PLA strongly depend on its thermal history, molecular weight, distribution, and purity. The melt flow index (MFI) of PLA is 12.48 g/10min, the average relative molecular weight of a PLA chip is 221,407.8 Da, the average molecular weight of a PLA chip is 123,120.4 Da, and the polymolecularity index (polydisperse coefficient) is 1.7983.

Process parameters

The spunbonding process parameters of concern were as follows: the polymer throughput rate, the polymer melt temperature, the primary air temperature, the venturi gap, and the air suction speed [35 - 37].To condense the discussions and comparison, a group of fundamental parameters was assumed during the computations: a polymer throughput rate of 0.15 g/min/hole, an initial temperature of the polymer melt of 195 °C, an initial air(primary) temperature of 15.6 °C, a venture gap of 30 mm, a suction speed of 220 m/s, a chamber length (L) of 3.4 m, and a spinneret hole diameter (D_0) of 0.45 mm. When one processing parameter was altered, the fundamental values of the other process parameters were held constant.

Test and methods

The image analysis method was employed to measure the fibre diameter. Images of nonwoven samples were acquired with a Questar three-dimensional video frequency microscope (Questar Corp., New Hope, PA) with an enlargement factor of 600 and a depth of focus of 1 mm, which were then processed with Image-Pro Plus image analysis software(Media Cybernetics, Inc., Silver Spring, MD) to measure the fibre diameter. The image processing includes enhancement, smoothing, binarisation and filtering. The size of the nonwoven fabric samples used on the university's equipment was 1 m × 1 m. Fibres of the spunbonded nonwoven are regarded as cylinders because their cross sections are nearly round. Twenty fibres were chosen to measure their diameters in each grid, so altogether there were 200 fibres measured in 10 grids. The mean value of the diameters of the 200 fibres was considered as the fibre diameter of the polylactic acid (PLA) nonwoven sample. During those experiments, these samples were held in a testing room maintained at 65% RH and 20 ± 5 °C; experiments were conducted after 24 hours.

The melt flow index (MFI) experiments on PLA were measured (performed) at a temperature of 180 °C, a load capacity of 2.160 kg, an aperture of the capillary tube of 2.095 mm, and at a length of the capillary tube of 8 mm on an RL---11B melt flow indexer at ambient temperature conditions of the room.

Numerical methods of solving the air jet flow field model of spunbonding

The air jet flow field model is solved by using the finite difference method. The SIMPLE algorithm is utilised to solve the problem of velocity pressure couple, and the staggered grid is presented to avoid tooth-like distributions of velocity and pressure. The difference scheme for space independent variables preferred is the second-order upwind difference scheme, and the TDMA method is used to solve the difference equations.

With the help of numerical simulations of the air jet flow field, we can determine the distributions of the z-component of the air velocity V_a and air temperature T_a along the axial position z. Then we can solve the air drawing model of the polymer using the fourth-order Runge-Kutta method. According our research, the initial air velocity is 70 m/s, the initial air temperature 15.6 °C, the polymer mass flow rate 0.15 g/min/hole, and the initial temperature of the polymer melt is 195 °C.

Results and discussion

Effect of the polymer throughput rate on the fibre diameter

Figure 1 shows the effect of the polymer throughput rate on the filament fibre diameter. As expected, lower polymer throughput rates yield finer fibres and more rapid attenuation. The filament fibre diameters change with the polymer throughput rate and vary from 0.1 g/min/hole to 0.4 g/min/hole. For the conditions in the figure, the final filament fibre diameter of 27.19 um at a polymer throughput rate of 0.4 g/min/hole is 28.4% larger than the final filament fibre diameter of 21.18 μm at a low polymer throughput rate (0.1 g/min/hole).There are two possible explanations for this: as the polymer throughput rate increased, the filament cooled more slowly along the spinline, which resulted in a larger final fibre diameter; or when the polymer throughput rate increased, the die entrance pressure

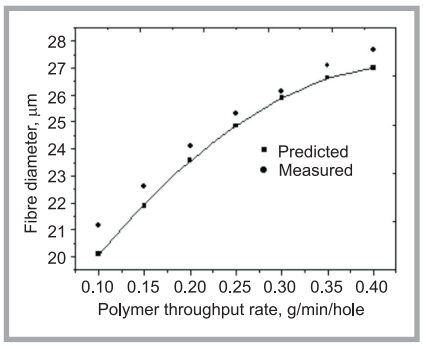

Figure 1. *Effect of the polymer throughput rate on the fibre diameter.*

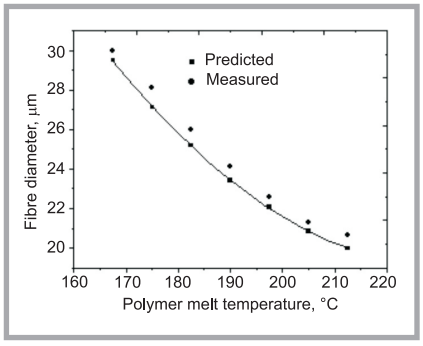

Figure 2. *Effect of the polymer melt temperature on the fibre diameter.*

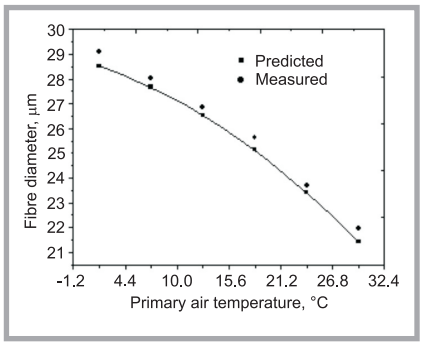

Figure 3. *Effect of the primary air temperature on the fibre diameter.*

increased, therefore the die swell increased. Due to this increase in the die swell at a higher throughput rate, the starting diameter was larger compared to that at a lower throughput rate. From all the analyses above, it can be concluded that reducing the polymer throughput rate can produce a finer fibre diameter.

Effect of the polymer melt temperature on the fibre diameter

Figure 2 reveals the effect of the polymer melt temperature on the filament fibre diameter. The higher the polymer melt temperatures, the finer the fibres are. A high polymer melt temperature (212.5 °C) results in a final filament fibre diameter of 20.58 μm, whereas a low polymer melt temperature (166.25 °C) results in a final filament fibre diameter of 30.17 μm. This was mainly due to the fact that at the lower polymer melt temperature, it may be difficult to extrude the polymer melt through the spinneret and achieve the final draw down; therefore it can be concluded that the effect of the polymer melt temperature was assessed in terms of the fibre diameter.

Effect of the primary air temperature on the fibre diameter

Figure 3 shows the fibre diameter changing with the primary air temperature. As expected, increasing the primary air temperature can produce a finer fibre diameter. Similar to the effect of the polymer melt temperature on the fibre diameter, a larger primary air temperature leads to the fibres being much more attenuated. When the primary air temperature increased from 1.67 °C to 29.5 °C, the fibre diameter decreased. The high primary air temperature (29.5 °C) results in a final filament fibre diameter of 21.98 μm, while the low primary air temperature (1.67 °C) results in a final filament fibre diameter of 29.11 μm. This may be explained by the following facts: firstly, the higher primary air temperature causes crystallization to occur much further from the spinneret, which leads to more drawing of filaments; secondly, an increase in the temperature of the primary air results in the viscosity of the polymer remaining at lower values for a greater distance from the spinneret, which causes a longer elapsed time. Because of the lower viscosity along the spinline, the final diameter and stress of the spinline decrease. Due to the decrease in stress, crystallisation starts at a much lower temperature, hence the final diameter decreases.

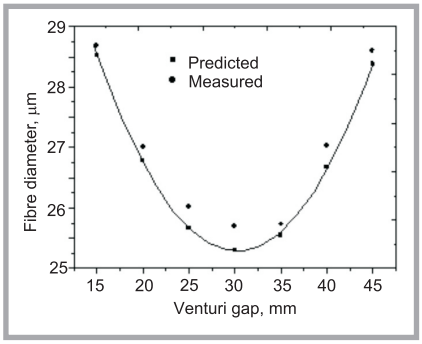

Figure 4. *Effect of the venturi gap on the fibre diameter.*

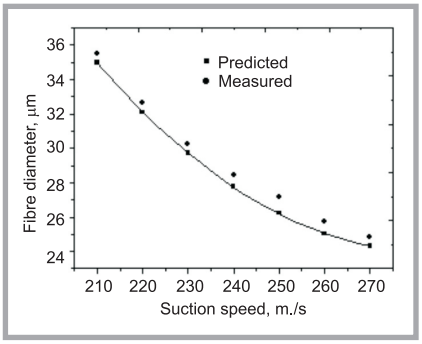

Figure 5. *Effect of the air suction speed on the fibre diameter.*

Effect of the venturi gap on the fibre diameter

Figure 4 presents the effect of the venturi gap on the final fibre diameter. As can be seen, the venturi gap opening changes with a varying quench pressure. The trend resulting from changing the mean fibre diameter by increasing the venturi gap is that the fibre diameter first decreased and then increased. It can also be seen from ***Figure 4*** that when the venturi gap increases from 15 mm to 45 mm, the quench pressure also changes. A low venturi gap **(**15 mm**)** and a high venturi gap (45 mm**)** can both produce a higher filament fibre diameter, whereas a medium venturi gap (30 mm) results in a minimum fibre diameter (25.39 μm), which indicates that with a 30 mm venturi gap the aerodynamic conditions may have been optimum to produce a finer filament fibre diameter. It can be concluded that a too high or too low venturi gap contributes little to the attenuation of the polymer fibre diameter as far as the polymer melt of PLA is concerned. This behaviour of the fibre diameter is in accordance with other researcher work [17], the fundamental reason is that the venturi gap controls the uniformity and laydown of the filaments onto the conveyor belt and, to a limited extent, the fibre diameter.

Effect of the air suction speed on the fibre diameter

Figure 5 illustrates how variations in the air suction speed cause changes in the fibre diameter. As is clear from ***Figure 5***, increasing the suction speed strongly reduces the fibre diameter over the range of suction speed observed. The high suction speed (270 m/s) results in a final filament fibre diameter of 24.34 μm, whereas the low suction speed (210 m/s) results in a final filament fibre diameter of 34.80 μm, which may be explained by the fact that the decrease in fibre diameter was due to the more drawing of filaments.

Experimental verification and combined parameter effects

Effects of combined polymer parameters (the polymer throughput rate and the initial temperature of the polymer melt) on the fibre diameter

Table 1 presents the measured and predicted fibre diameters when the initial(primary) air temperature (12.8 °C) and the initial air speed (80 m/s) are kept unchanged, while the polymer throughput rate, and the initial temperature of the polymer melt are varied, where the fibre diameters predicted agree with those measured. ***Table 1*** reveals that a lower polymer throughput rate, and a higher initial temperature of the polymer melt will yield finer fibres. Therefore, it is concluded that the polymer throughput rate and initial temperature of the polymer melt are key factors in the controlling of the final diameter of the filament fibre.

Table 1*. Effects of combined polymer parameters(polymer throughput rate and initial temperature of the polymer melt) on the fibre diameter.*

No.	Polymer throughput rate, g/min/hole	Initial temperature of polymer melt, °C	Initial air temperature, °C	Initial air speed, m/s	Measured diameter, μm	Predicted diameter, μm	Prediction error, %
1	0.24	205	12.8	80	23.18	22.12	4.56
2	0.15	205	12.8	80	21.04	20.27	3.34
3	0.36	205	12.8	80	24.60	23.07	6.20
4	0.24	195	12.8	80	23.41	22.25	4.93
5	0.24	220	12.8	80	22.54	20.74	8.00

Table 2. Effects of combined air parameters (initial air temperature and initial air speed) on fibre diameter.

No.	Polymer throughput rate, g/min/hole	Initial temperature of polymer melt, °C	Initial air temperature, °C	Initial air speed, m/s	Measured diameter, μm	Predicted diameter, μm	Prediction error, %
1	0.24	220	12.8	70	21.19	20.22	4.58
2	0.24	220	11.4	70	24.89	23.50	5.58
3	0.24	220	15.6	70	20.20	19.19	5.02
4	0.24	220	12.8	60	23.51	22.29	5.19
5	0.24	220	12.8	80	21.48	20.20	5.98

Effects of combined air parameters (the initial air temperature and initial air speed) on the fibre diameter

Table 2 gives the measured and predicted fibre diameters. When the polymer throughput rate (0.24 g/min/hole) and the initial temperature of the polymer melt (220 °C) are held at a constant level, the initial air temperature and initial air speed are changed, the fibre diameters predicted tally well with those measured. ***Table 2*** also shows that increasing the initial air temperature and initial air speed can decrease the filament fibre diameter. It is concluded that the initial air temperature and the initial air speed have a very important influence on fibre diameters. The study results also indicate that the air drawing model of polymers we established can predict the drawing effects of the nonwoven spunbonding process.

By observation it was concluded that the fibre diameters predicted are much closer to the experimental data measured, which further confirms the effectiveness of the polymer drawing model established in this work. From the analyses above, it can be seen that the fibre diameter is directly related to the polymer throughput rate, the initial temperature of the polymer melt, the initial air temperature and the initial air speed, i.e., the finer the geometric mean of the fibre diameter, the more uniform the fibre web will be.

Conclusions

A polymer air drawing model of PLA spunbonding nonwovens has been established. The effects of spunbonding processing variables, including the polymer throughput rate, the initial temperature of the polymer melt, the primary air temperature, the initial air speed, the venturi gap and the air suction speed on the final filament fibre diameter have been investigated. A lower polymer throughput rate, a higher polymer melt temperature, a higher initial air velocity, a higher primary air temperature of the polymer, a higher air suction speed, and a medium small (or higher) venturi gap can all produce a finer filament fibre diameter, which can encourage us to further study how fine a filament fibre diameter can be obtained for the spunbonding process and what factors influence the filament fibre diameter. It can be concluded that variation in the density and specific heat capacity of the polymer melt at constant pressure and temperature has a great effect on the fibre diameter. Therefore, the model predictions can be improved dramatically when the influences of the polymer temperature on the density and specific heat capacity of the polymer melt at constant pressure are considered. Compared with the existing drawing model, the new ones include more processing parameters and are more accurate. The newly developed formulas have been incorporated into a theoretical model of spunbonding to predict the fibre diameter of nonwoven webs. The results predicted are in quite good agreement with the data actually measured, which shows that the new air drawing model is effective and excellent. At the same time, the experimental results also demonstrate the great potential of this research for use in the computer-aided design of spunbonding technology.

References

1. Malkan, S. R.; Tappi 1994 Nonwovens Conference, pp. 31-37 (1994).
2. Lu, F. M.; Tappi 1998 Nonwovens Conference, pp. 125-132 (1998).
3. Bhat, G. S., Malkan, S. R.; J. Appl. Polym. Sci., 83, 3, pp. 572-585 (2002).
4. Smorada, R. L.; INDA J. Nonwovens Res., 3, 4, p. 26 (1991).
5. Kothari, V. K.; The Indian Textile Journal, 46, 2, pp. 17-24 (2004).
6. Lewandowski Z., Ziabicki A., et al.; Fibres & Textiles in Eastern Europe, 15, 5-6 (64-65), pp. 77- 82 (2007).
7. Qu, Y.-H.; Proceed. of The Textile Institute 83rd World Conf., pp. 1056-1059 (2004).
8. Linnemann, B., et al.; Chemical Fibres International, 53, pp. 426-433 (2006).
9. Hagen, R.; Chemical Fibres International, 50, pp. 540-542 (2000).
10. Bogaert, J. C., Coszach, P.; Nonwovens World, 9, pp. 83-91 (2000).
11. Woodings, C.; Nonwovens World, 10, 2, pp. 71-78 (2001).
12. Lunt, J.; Int. Fibre J., 15, 3, pp. 48-52 (2000).
13. Matsui, M., Kondo, Y.; Chemical Fibres International, 46, p. 318 (1996).
14. Lunt, J., Shafer, A.; Journal of Industrial Textiles, 29,pp. 191-205 (2000).
15. Sawyer, D. J.; Nonwovens World, 10, 2, pp. 49-53 (2001).
16. Dugan, J. S.; Int. Nonwovens J., 10, 3, pp. 29-33 (2001).
17. Lunt, J.; Technical Textiles Int., 9, 10, pp. 11-13 (2000).
18. Wojciechowska E., Fabia J., Slusarczyk Cz., Gawlowski A., Wysocki M., Graczyk T.; Fibres & Textiles in Eastern Europe, 13, 5(53), pp. 126-128 (2005).
19. Zachara A., Lewandowski Z.; Fibres & Textiles in Eastern Europe, 16, 4(69), pp. 17-23 (2008).
20. Jarecki L., Ziabicki A.; Fibres & Textiles in Eastern Europe, 16, 5(70), pp. 17-24 (2008).
21. Jarecki L., Lewandowski Z.; Fibres & Textiles in Eastern Europe, 17, 1(72), pp. 75-80 (2009).
22. Malkan, S. R., et al.; Int. Nonwovens J., 6, 2, pp. 24-50 (1994).
23. Chen, C. H., et al.; Textile Res. J., 53, 1, pp. 44-51 (1983).
24. Beyreuther, R., Malcome, H. J.; Melliand Textilber., 74, 4, pp. 287-289 (1993).
25. Hajji, N., Spruiell, J. E.; INDA J. Nonwovens Res., 4, 2, pp. 16-21 (1992).
26. Misra, S., Spruiell, J. E.; INDA J. Nonwovens Res., 5, 3, pp. 13-19 (1993).
27. Gagon, D. K., et al.; Polym. Eng. Sci., 21, 13, pp. 844-853 (1981).
28. Ziabicke, A., Kawai, H.; "High-speed fibre spinning science and engineering aspects", John Wiley & Sons, Inc., 1985.
29. Guo, D.-S., Wang, W.-K.; China Textile Press, Beijing, China, 2001.
30. Oh, T., Polym. Eng. Sci., 46, 5, pp. 609-616 (2006).
31. Cao, J. N. Takeshi K.; J. Appl. Polym. Sci., 32, 5, pp. 2683-2697 (1988).
32. Bhuvanesh, Y. C., Gupta, V. B.; J. Appl. Polym. Sci., 58, 3, pp. 663-674 (1995).
33. Takeshi, K.; J. Appl. Polym. Sci., 62, 8, pp. 1913-1924 (1996).
34. Zieiminski, K. F., and Spruiell, J. E.; Synthet. Fibres, 25, 4, 1986, pp. 1-36.
35. Mastui, M.; Trans. Soc. Rheol., 20, 3, pp. 465-467 (1976).
36. Abbott, L. E., White, J. L.; Appl. Polym. Symp., 20, pp. 247-268 (1973).
37. Bankar, V. G., et al.; J. Appl. Polym. Sci., 21, pp. 2135-2155 (1977).
38. Patel, R. M., Spruiell, J. E.; Polym. Eng. Sci., 31, 6, pp. 730-736 (1991).
39. Smith, A. C.; Int. Nonwovens J., 6, 1, pp. 31-41 (1994).
40. Jeon, B. S.; Textile Res. J., 71, 6, pp. 509-513 (2001).
41. Miller, C.; AIChE J., 50, 5, pp. 898-905 (2004).

Received 12.01.2009 Reviewed 17.08.2009